CCD characterization for astronomy space missions at ESA

P. Verhoeve[a1], T. Prod'homme[b] , T. Oosterbroek[a], N. Boudin[a], L. Duvet[a]
[a]Future Missions Preparation Office, Directorate of Science and Robotic Exploration, ESTEC/ESA
[b]Opto-electronics Section, Directorate of Technical and Quality Management, ESTEC/ESA

ABSTRACT

ESA's astronomy missions make wide use of CCDs as their main photon detectors. Depending on the scientific goals of the mission, different aspects the CCD's performance may be critical for the achievement of these goals. The Payload Technology Verification section of ESA's Future Missions Preparation Office has a task to provide support on issues related to payload performance. For that purpose we operate a versatile CCD test bench. We present test results on CCDs for missions that are currently under study (PLATO) or under development (EUCLID, CHEOPS).

Keywords: CCD, astronomy

1. INTRODUCTION

Many of the European Space Agency's (ESA) astronomy missions, whether in operation, under development, or under study, rely on CCDs as their principal detectors. In most cases, even if instruments are provided by external PI-led consortia, ESA takes responsibility for the procurement of the CCDs in these instruments.

An example of a mission in operation is XMM-Newton (launched in 1999), where both the Reflection Grating Spectrometer (RGS) [1], and the focal plane imager (EPIC) [2] are using back- and front-illuminated CCDs, respectively, from e2v. More recently, GAIA, ESA's high precision astrometry mission, was launched into an L2 orbit at the end of 2013, carrying a focal plane of 106 CCDs with a total sensitive area of 2800 cm^2. An overview of this focal plane, including some early results from the in-flight commissioning is given in [3].

The Euclid mission, currently under development, is designed to measure the expansion history of the Universe and the growth of cosmological structures, and understand the origin of Universe's accelerating expansion. For this purpose it uses two cosmological probes, Weak Lensing and galaxy clustering. The mission will observe galaxies and clusters of galaxies out to a red-shift of z~2, in an all-sky survey covering 15000 deg². It consists of a 1.2m diameter Korsch telescope with two focal plane instruments: a visual imager (VIS) and a near-IR spectro-photometer (NISP). Both instruments share a common field of view of 0.55 $degrees^2$. Euclid will be launched in 2020, for 6 years of operation at the Sun-Earth L2 point. A further description of the Euclid mission, currently at the beginning of phase B2, is given in Laureijs et al. [4]. The VIS instrument consists of a CCD-based focal plane array, with a shutter mechanism to close the optical path during read out and dark calibration, and a calibration unit for flat field measurements. It covers the wavelength range of ~550-920 nm as a single wide band. The FPA supports 6×6 CCDs (4k×4k pixels each) with a plate scale of 0.1 arcsec/pixel giving a geometric field of 0.55 deg^2 (including the gaps between the CCDs). With the weak lensing technique, the VIS channel measures the shapes of galaxies with about 0.16 arcsec (FWHM) system point-spread function. This technique requires an unprecedented accuracy to which the shapes of the galaxies have to be measured. In particular, radiation damage effects in the CCDs will challenge this accuracy during the mission. A detailed description of the VIS instrument can be found in Cropper et al. [5].

The PLATO space mission (PLAnetary Transits and Oscillation of stars) [6] was selected early 2014 as ESA's M3 mission in the Cosmic Vision program, and has just entered the definition study phase. PLATO will detect terrestrial exoplanets in the habitable zone of solar-type stars and characterise their bulk properties. It will provide the key information (planet radii, mean densities, stellar irradiation, and architecture of planetary systems) needed to determine the habitability of these planets. The tools for these science objectives will be photometry and astroseismology, enabled by a single instrument that will be provided by the PLATO Mission Consortium. The instrument consists of 32 "normal" telescopes with CCD based focal planes, operating in white light and providing a very wide field of view (FoV). They will be read out with a cadence of 25 s and will monitor stars with mV > 8. Two additional "fast" cameras with high

[1] Email: peter.verhoeve@esa.int

High Energy, Optical, and Infrared Detectors for Astronomy VI, edited by Andrew D. Holland, James Beletic, Proc. of SPIE
Vol. 9154, 915416 · © 2014 SPIE · CCC code: 0277-786X/14/$18 · doi: 10.1117/12.2058110

read-out cadence (2.5 s) will be used for stars with mV ~4–8. The cameras are based on a fully dioptric design with 6 lenses. Each camera has an 1100 deg^2 FoV and a pupil diameter of 120 mm and is equipped with a focal plane array of 4 CCDs each with 4510^2 pixels of 18 μm size, working in full frame mode for the "normal" camera and in frame transfer mode for the "fast" cameras. The mission will be able to cover about 50% of the sky in survey mode during the nominal observing time. Plato is scheduled to be launched in 2024 for a 6 year nominal mission into an L2 orbit.

As a last example, we mention CHEOPS (CHaractererising ExOPlanet Satellite) [7], the first small (S-class) mission in the Cosmic Vision program. The main science goals of the CHEOPS mission will be to measure the bulk density of super-Earths and Neptunes orbiting bright stars and provide suitable targets for future in-depth characterisation studies of exoplanets in these mass and size ranges. To reach its science objectives, CHEOPS will be able to detect an Earth-size planet transiting a G5 dwarf star of 0.9 RSun with $6 \leq mV \leq 9$. Since the depth of such a transit is 100 ppm, this requires a photometric precision of 20 ppm in 6 hours of integration time, which corresponds to the transit duration of a planet with a revolution period of 50 days. This precision will be achieved by using a single, frame-transfer, back-illuminated CCD detector with 1024×1024 pixels and a pixel pitch of 13 μm. The detector will be mounted in the focal plane of a ~33 cm diameter, f/8, on-axis Ritchey-Chrétien telescope; it will be passively cooled to < 233 K, with thermal stability < 10 mK. After a <4 year development time, CHEOPS will be launched in 2017 into a sun-synchronous low-earth orbit for a nominal mission duration of 3.5 years.

In most of the above missions, whether the instruments are provided by ESA or by an instrument consortium, the CCDs in these instruments are usually developed and procured under ESA's responsibility. In order to provide support to the development and characterization programs and to enable an independent assessment of the detectors, we have developed an in-house test bench for CCDs. In the next paragraphs we discuss our specific role in ESA's science program, and we show test results on CCDs for the EUCLID, CHEOS and PLATO missions.

2. PAYLOAD TECHNOLOGY VALIDATION ACTIVITIES

The Payload Technology Validation section (SRE-FV) in the Science and Robotic Exploration directorate is providing support to present and future missions at different stages in their lifetime. The main tasks are:
- support to SRE-F (Future missions): the main goal is to validate the technology for future missions in order to de-risk the overall program before the mission adoption (occurring at the end of phase B1). The synergy between the mission study team, the Technology Development Activity technical officers and the test team is optimised. A first example was EUCLID with its CCD273 for VIS and the Hawaii-2RG detector for NISP. More recently, with the selection of PLATO as M3 mission, we will also support the development of the instrument CCDs.
- support to SRE-P (Projects): projects in development are requesting specic tests to be performed to insure control of some performances under ESA responsibility or affecting items under ESA responsibility. EUCLID is now in this configuration, and we continue to support the EUCLID project and the VIS instrument team with mission performance related tests
- support to SRE-O (Operation): these activities are dedicated to missions in operation with essentially cross-validation on ground of effects or issues observed in instruments on board. A typical example is GAIA, for which a dedicated CCD test bench (not discussed in this paper), built and previously operated at Airbus Defence and Space (Toulouse, France), is now operated in our laboratories. This bench has already provided valuable contributions to the GAIA focal plane commissioning phase.
- With limited resources, support is also given to SRE-S (Science) scientists with the implementation of small research programs with internal funding, the latest example is the DECA (Descent Camera) camera delivered to the EXOMARS project.

Due to the long-term heritage of the Science and Robotic Exploration laboratories, most of these activities are presently focusing on detector technology, however on the long-term, the scope could become broader. Descriptions of our test facilities for CCDs and infrared detectors can be found in [8], [9], [10].

3. DESCRIPTION OF THE CCD TEST BENCH

A detailed description of our CCD test facility is given in [8]. In short, the bench hosts a liquid nitrogen cooled cryostat with a temperature controlled CCD stage (T=120-300K). This stage can hold a single CCD in formats up to 8x8 cm^2 and also carries a 4 channel Front End Electronics board (XCAM ltd, UK) (Figure 1). The cryostat has a fused silica, AR

coated vacuum window for optical illumination. The source can be either an uniformly illuminating Integrating Sphere, fed with tunable (350-1050nm) monochromatic light from a grating monochromator (see Figure 2), or projectors (for sub pixel size spots or masks with arbitrary scenes) mounted on 3-axis precision translation stages. Alternatively, the vacuum window can be exchanged for a metal flange that carries a radioactive ^{55}Fe source with commandable shutter, which allows for x-ray illumination with 5.9 keV photons.

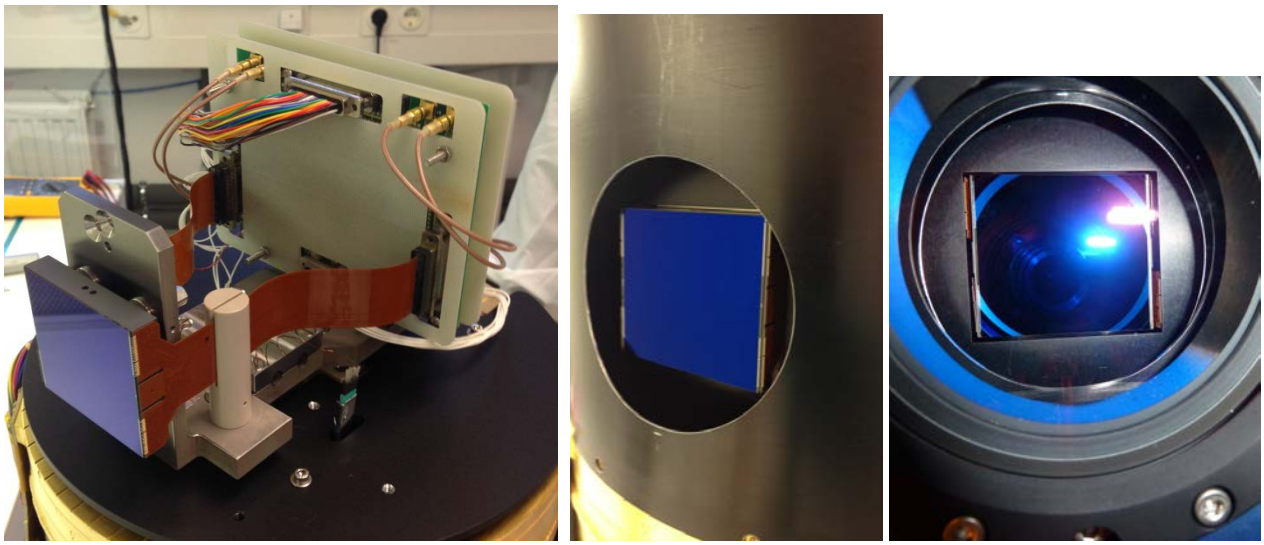

Figure 1: Left: CCD273 and 4-channel headboard on cold stage, middle: with shields, right, seen through the vacuum window.

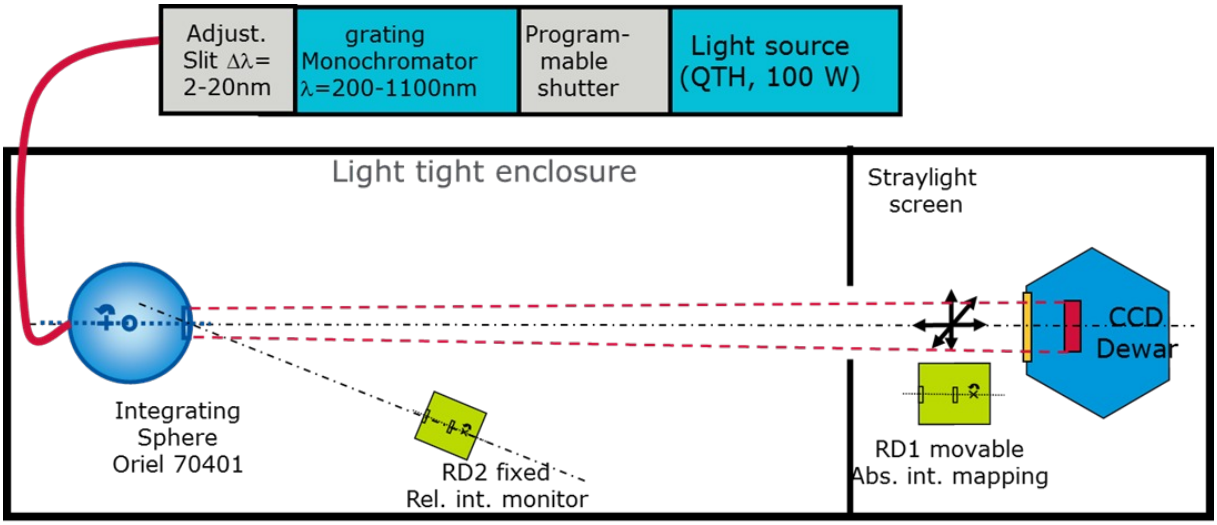

Figure 2: schematic of the uniform illumination setup (see text for further details).

For Quantum Efficiency measurements, the output beam of the integrating sphere is collimated with apertures at the sphere output port and immediately in front of the calibrated photodiode (see Figure 3). The geometry is chosen such that the resulting spot on the photodiode is smaller than the sensitive area of the diode, and smaller than the CCD sensitive area as well. This warrants that the number of photons registered on the reference photodiode and on the CCD are the same, apart from the finite transmission of the cryostat window. This configuration thus avoids uncertainties related to extrapolations the intensity distribution at the positions of the reference detector and the CCD, which are needed in case of full illumination of the CCD. On the downside, the QE measurement is now local, and the intensity varies across the spot on the CCD. The procedure consists of an intensity versus wavelength measurement with the calibrated photodiode in the beam, followed by a similar measurement with the CCD (after removal of the photodiode from the beam). A

second photodiode (photodiode 2 in Figure 3), operated during both scans, allows for corrections for intensity variations during the two scans.

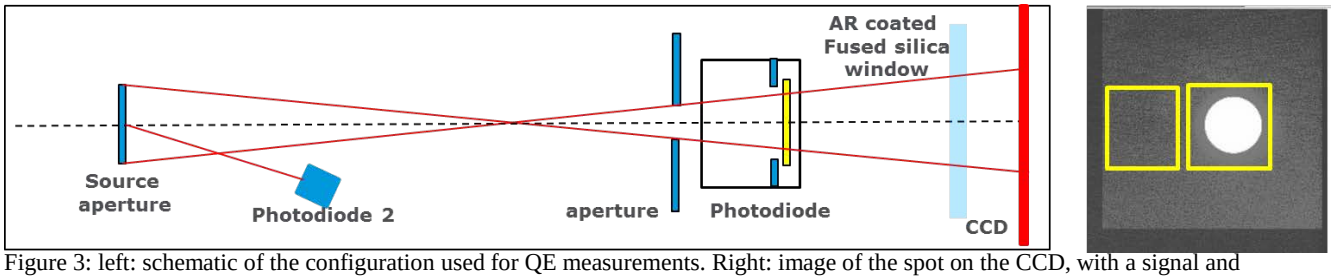

Figure 3: left: schematic of the configuration used for QE measurements. Right: image of the spot on the CCD, with a signal and reference boxes superimposed.

The CCD controller (from XCAM ltd, UK), provides bias voltages and clocks from separate bias and clock driver cards. Clocks and Correlated Double Sampling (CDS) timing sequences with a time resolution of about 30 ns are generated from an ADSP 2181 chip on the clock driver card. The pixel rate is limited to <1 MHz. The video signals from the CCD are pre-amplified (3x) on the FEE electronics board in the cryostat, and then fed into a 4-channel Dual Slope Integrator CDS/ADC card with a 16-bits ADC chip. The CCD test bench is controlled via a dedicated Python script. Devices and processes under control of the Python application are: the CCD controller, CCD and FEE temperature controller, temperature readout, monochromator wavelength setting and filter selection, shutters, translation stages and power read out from reference photodiodes. The control software allows for a high degree of automated measurement series through nested loops of parameter variations.

4. CCDS FOR EUCLID: CCD273

4.1 CCD273 description

The CCD 273-84-2-F15 is a Back-illuminated Euclid format device delivered to ESA as part of the Euclid CCD predevelopment contract. It has 4k x 4k pixels, divided in two halves with a charge injection structure in the middle. Each of the two read-out registers has two output nodes, one at either end (Figure 4). It is based on the existing CCD203-82 design with some changes and trade-offs to optimize performance :

- there is only one output gate at the end of each read-out register, which eliminates the option of gain switching
- the width of the register channel has been reduced to improve the radiation hardness of the device
- a parallel charge injection structure is included in the middle of the image area,
- high resistivity silicon and thin gate dielectric processes are used.
- The output amplifier is derived from CCD231, and combines low noise and high responsivity (~7-8 µV/e-).

Table 1: Specifications for the EUCLID CCD273

parameter	specification	remarks
Image format	4kx4k, Full Frame, 4-phase image areas, 3-phase registers	5x5 cm^2 sensitive area, two independently clocked image areas, separated by a charge injection structure
Pixel size	12x12 μm^2	
Operating mode	Back-illuminated, non-inverted	Back-thinned to 40 µm
Amplifier responsivity	6-8 µV/electron	2 registers, 4 amplifiers
Read noise	<3.6 electron rms	@ 70 kHz pixel rate
Full Well Capacity	> 175 k electrons	
Charge Transfer Inefficiency (CTI)	$<5\times10^{-6}$	@ T=153K, E=5.9keV, 1 photon/80 pixels
Dark signal	$<6\times10^{-4}$ electrons/pixel/s	@ T=153K
Quantum efficiency	>83%, >83%, >23%	@ 550, 750 and 950nm

The read-out register has a gate controlled dump drain to allow fast dumping of unwanted data. The SiC package provides guaranteed flatness at cryogenic temperatures, as well as a compact footprint. Connections are made at the top and bottom of the device, so that the sides may be close butted if needed. The end-bonded flexis at the top and bottom are made such that close butting is also possible at the end-to-end side. The main specifications of the CCD are listed in Table 1. Further details can be found in [11].

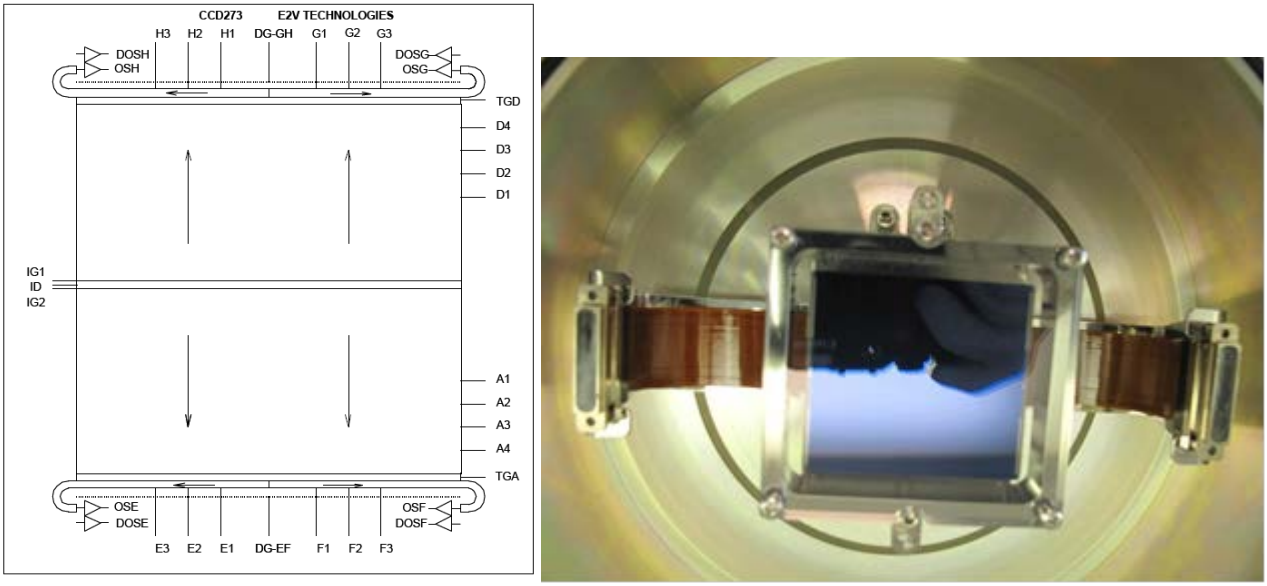

Figure 4: left: schematic of the CCD273 (seen from the back-thinned side). Right: a CCD273 in its handling/transportation jig with protective cover.

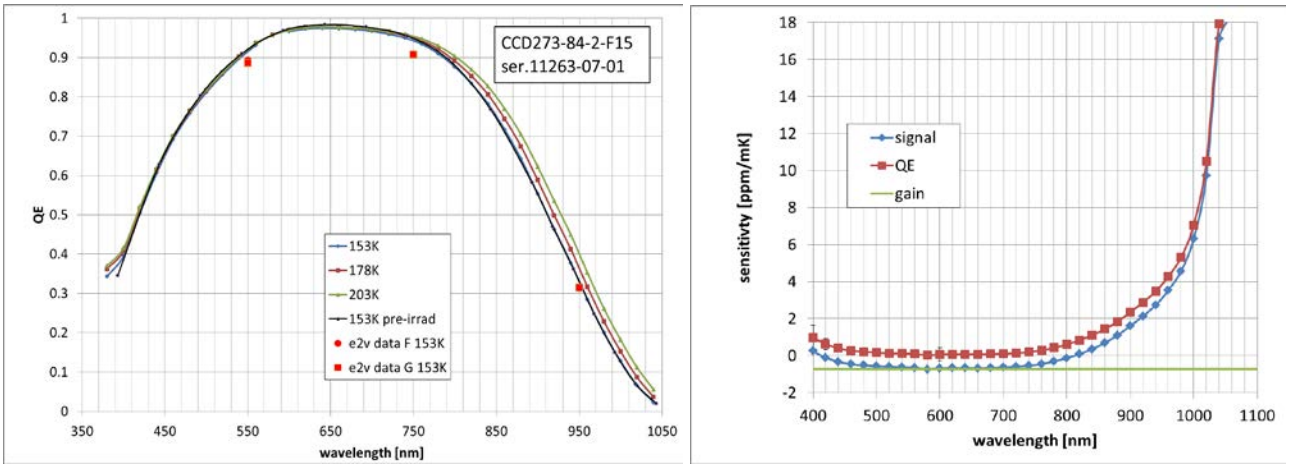

Figure 5: left: measured QE at 3 different temperatures. The red dots represent e2v measurements. Right: temperature sensitivity of QE, gain and signal at T=178K.

4.2 Test results

Basic performance characterization of this CCD has been reported elsewhere [12]. Additional quantum efficiency measurements at different temperatures are shown in Figure 5. The uncertainties on the absolute QE values are estimated at 3%. Gain values needed to derive the absolute QE have been derived from photon transfer curves measured at the different temperatures, and also from 5.9 keV X-ray measurements. Gain values derived from these two methods are found to be in agreement to within 1%. The expected decrease of QE at longer wavelengths for decreasing temperature is confirmed. From the QE values for 3 different temperatures, we derive the sensitivity of the QE (in ppm/mK) for

temperature variations at the middle value of the 3 temperatures (178K), see right panel of Figure 5. Also shown is the sensitivity of the gain, which is found to be -0.72 ppm/mK (at 178K). Combination of gain and QE sensitivity yields the sensitivity of the measured signal, which would be the important parameter in a photometry noise budget.

In the context of the EUCLID mission, CCD testing in the VIS instrument consortium is concentrating on characterization and mitigation of radiation damage effects [13][14][15]. Our contribution to this work is aiming at the direct measurement of changes in the measured shapes (expressed in ellipticities) of galaxies projected on the CCD.
For this purpose, the CCD has been irradiated at room temperature with 10 MeV protons at a flux of the 9.0×10^6 protons cm^{-2} s^{-1} at the accelerator of the Kernfysisch Versneller Instituut (Groningen, The Netherlands). Two different illumination masks were used, corresponding to region I (total dose 2.4×10^9 protons) and regions II and III (total dose 4.8×10^9 protons), respectively (see Figure 6). The latter dose is the expected End-of-Life (EOL) dose after the 6 years mission. Irradiation of regions I and II includes the serial registers, whereas the serial register for region III was masked. This irradiation scheme, together with the flexibility in readout directions through the 4 readout nodes, allows for multiple options to measure the degradation of charge transfer efficiency.

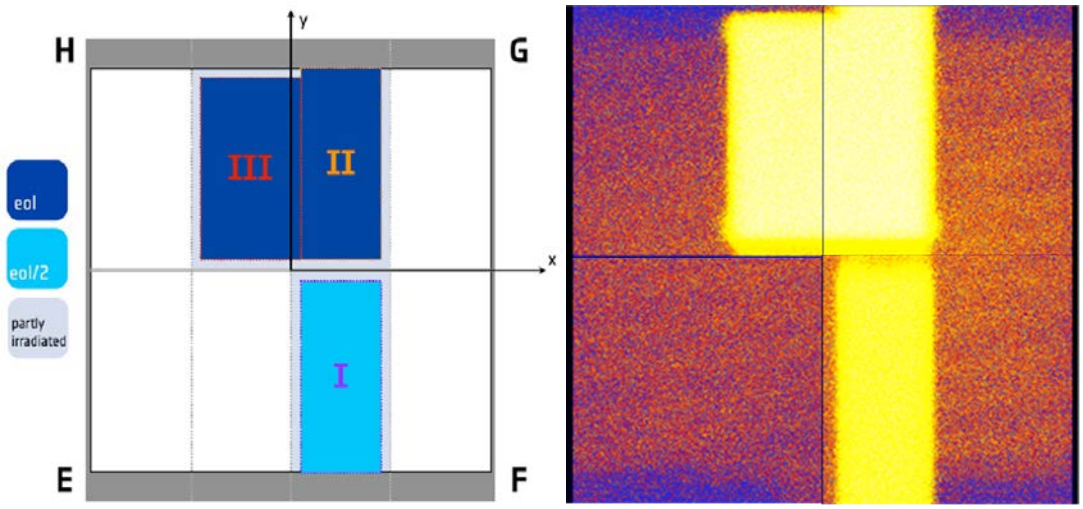

Figure 6: left: schematic of the irradiation scheme. Right: 1000s dark image at T=243K, showing the enhanced dark signals in the irradiated regions.

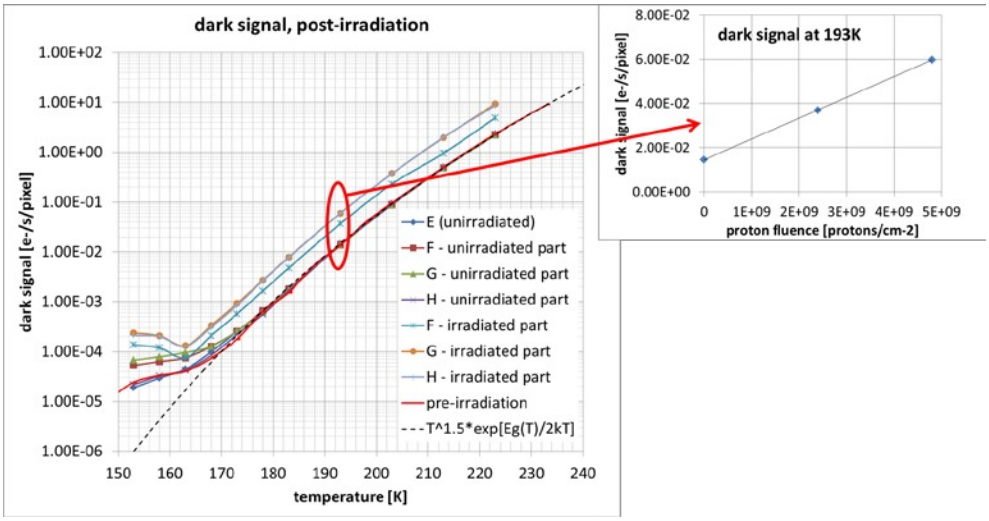

Figure 7: Measured dark signal (pre- and post-irradiation) for the various (un-)irradiated sections. The inset shows the proportionality of dark signal increase (at T=193K) with radiation dose.

Results of dark signal measurements in the various sections of the CCD are collected in Figure 7. The results for all un-irradiated areas, pre- and post-irradiation, are undistinguishable, as are the results for the equally irradiated sections II and III. The increase in dark current is found proportional to the radiation dose.

The results of Charge Transfer Efficiency (CTI) measurements as a function of temperature using 5.9 keV X-rays are shown in Figure 8. The relevant operating conditions are: pixel rate 70 kHz (with equal phase-high durations of the three serial phases), a line transfer time of 0.11 ms, and the standard two-level clocking for both serial and parallel clocks. Clearly, a low operating temperature is favorable for mitigation of the radiation induced degradation of CTI, hence the choice of 153K for Euclid. The results at T=153K are summarized in the bottom panel of Figure 8, which shows serial and parallel CTI versus proton dose. The slopes of these lines, referred to as the radiation damage constants, are found as 5.4×10^{-15} cm^2 and 9.8×10^{-15} cm^2, for serial and parallel transfer, respectively. These numbers are in fair agreement with values found by Gow et al [14] for a front-illuminated (but otherwise identical) Euclid prototype CCD, at slightly different operating conditions (160K, 200kHz pixel rate).
A detailed comparison of CTI measurements and trap densities derived from different test methods (X-rays, Extended Pixel Edge response, First Pixel response and trap pumping) [16], as well as results of a laboratory simulation of the effects of CTI degradation on measured galaxy shapes [17] are given elsewhere in these proceedings .

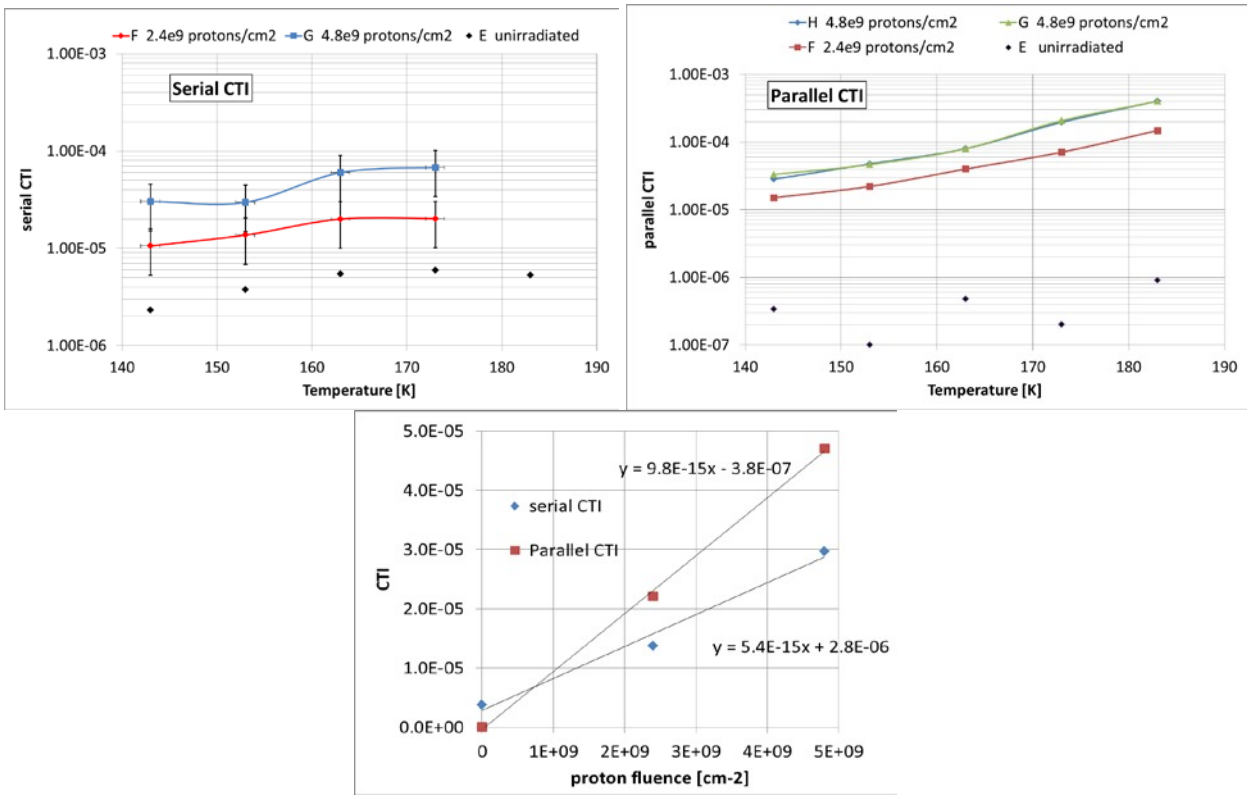

Figure 8: Measured serial (top left) and parallel (top right) CTI, post-irradiation, versus temperature for two irradiated sections. The black diamonds in the lower decade show the pre-irradiation values. Bottom: dependence of CTI (T=153K) on proton dose.

5. CCDS FOR PLATO: CCD270

5.1 CCD270 description

The CCD 270-84-2-F15 (e2v Technologies) is a Back-illuminated PLATO format device delivered to ESA as part of the PLATO CCD predevelopment contract. It has 4510 x 4510 pixels, divided in two independently clocked halves, allowing for frame transfer mode operation (see Figure 9). The read-out register has two output nodes, one at either end. Low resistivity silicon and thin gate dielectric processes are used. The read-out register has a gate controlled dump drain

to allow fast dumping of unwanted data. The device has a SiC package and a single flex cable for all bias, clock and signal connections. The main specifications of the CCD are listed in Table 2. A more detailed description of this CCD can be found in [18]. The nominal operating conditions for PLATO will be a pixel rate of 4 MHz per output node with <28 electrons rms readout noise, and an operating temperature of 203K.

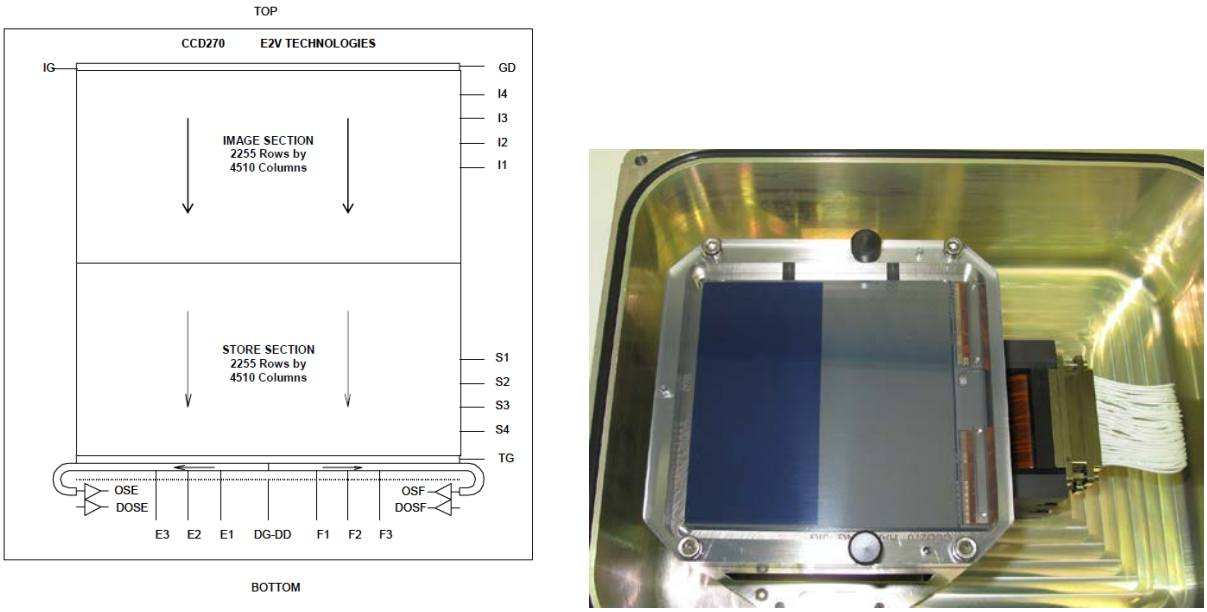

Figure 9: Left: schematic of the CCD270 (Frame Transfer version). Right: photograph of the Frame Transfer version of CCD270

Table 2: Specifications for the PLATO CCD270

parameter	specification	remarks
Image format	4.5kx4.5k, Full Frame or Frame Transfer, 4-phase image areas, 3-phase registers	8x8 cm^2 sensitive area
Pixel size	18x18 μm^2	
Operating mode	Back-illuminated, non-inverted	Back-thinned to 16 µm
Amplifier responsivity	2 µV/electron	1 register, 2 amplifiers
Read noise	<28 electron rms	@ 4 MHz pixel rate per output
Full Well Capacity	> 900 k electrons	
Charge Transfer Inefficiency (CTI)	$<1\times10^{-5}$	@ 4 MHz and T=203K
Dark signal	<1.2 electrons/pixel/s	@ T=203K
Quantum efficiency	>73.7%, >85.8%, >31.4%	@ 500, 700 and 900nm

5.2 Test results

Our test bench does not yet allow for operation of the device at the nominal pixel rate of 4 MHz per output node. Therefore, basic performance has been tested at 70 kHz, using timing files available from the testing of the EUCLID CCD273. Results are:

- Read noise ~4.0 electrons rms for both amplifiers (at 70 kHz pixel rate)
- Serial CTI =3.1×10^{-6} (70 kHz pixel rate, T=153K)
- parallel CTI =4×10^{-7} (70 kHz pixel rate, T=153K)
- dark current = 0.6 electrons/pixel/s at T=203K
- global Pixel Response Non-Uniformity (PRNU) <0.6% rms at λ=700nm

The main goal of the test was the verification of the QE values as reported by e2v. Results of quantum efficiency measurements at different temperatures are shown in Figure 10. The uncertainties on the absolute QE values are estimated at 3%. Gain values needed to derive the absolute QE have been derived from photon transfer curves measured

at the different temperatures. The expected decrease of QE at longer wavelengths for decreasing temperature is confirmed. From the QE values for 3 different temperatures, we derive the sensitivity of the QE (in ppm/mK) for temperature variations at the middle of the 3 temperatures (178K), see right panel of Figure 10. Also shown is the sensitivity of the gain, which is found to be -0.73 ppm/mK (at 178K). Combination of gain and QE sensitivity yields the sensitivity of the measured signal, which will be an important parameter in the photometry noise budget for PLATO.

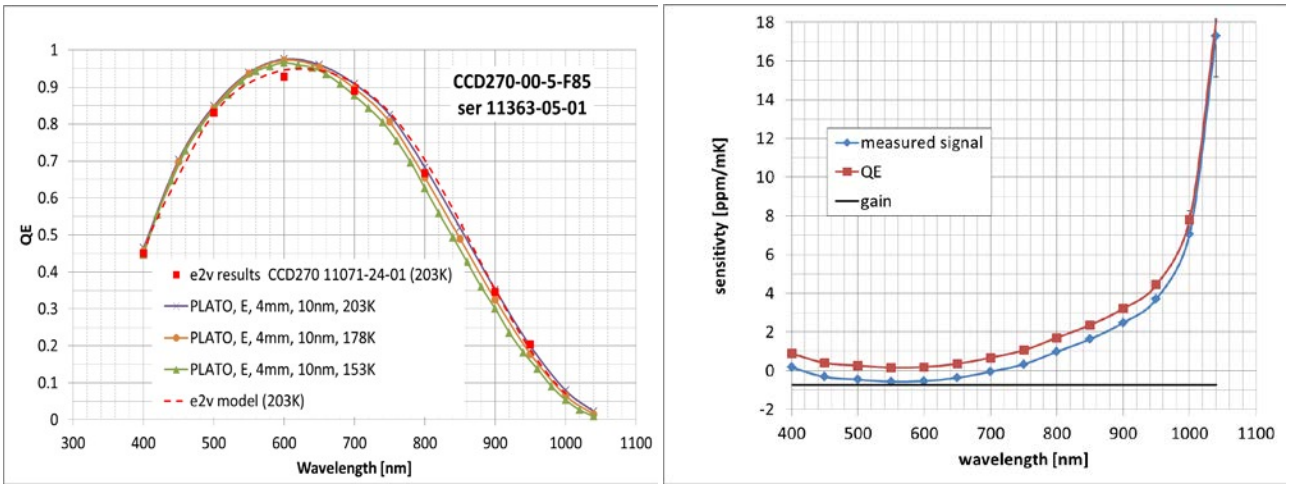

Figure 10: left: measured QE at 3 different temperatures. The red dots represent e2v measurements. Right: temperature sensitivity of QE, gain and signal at T=178K.

Further tests planned for the near future involve proton irradiation of a CCD270 and evaluation of the CTI degradation at the relevant pixel rate and operating conditions. For this purpose, we will upgrade our CCD controller for operation at 4MHz pixel rate with sufficiently low read noise. In addition we plan to map intra-pixel responsivity variations, using a spot projector with sub-pixel sized spot at several wavelengths [8].

6. THE CCD FOR CHEOPS: CCD47-20

6.1 CCD47-20 description

Since the short duration of the implementation program of the CHEOPS mission excludes any new technology developments, the photometer instrument will use the existing CCD47-20 device of e2v Technologies. This device is a 1kx1k back-illuminated Frame Transfer CCD, that will be operated with 200 kHz pixel rate at T=233K for integration times of up to 60s. The inverted mode version of the CCD47-20 will be used in order to achieve a negligible contribution of the dark current to the overall noise budget. Specifications relevant for CHEOPS are listed in Table 3. Further details are found in the data sheet available from e2v Technologies.

Table 3: Specifications for the CCD47-20 applicable to CHEOPS

parameter	specification	remarks
Image format	1kx1k, Frame Transfer, 3-phase	1.3x1.3 cm^2 sensitive area,
Pixel size	13x13 μm^2	
Operating mode	Back-illuminated, inverted mode	Back-thinned to 12 µm
Amplifier responsivity	3-4 µV/electron	1 registers, 2 amplifiers
Read noise	<6 electron rms	@ 200 kHz pixel rate
Full Well Capacity	> 60 k electrons	
Charge Transfer Inefficiency (CTI)	$<5\times10^{-6}$	@ T=233K, E=5.9keV
Dark signal	<0.1 electrons/pixel/s	@ T=233K
Quantum efficiency	>85%, >80%, >26%	@ 500, 700 and 900nm

6.2 Test results

The CCDs for the CHEOPS qualification and flight program are currently in fabrication, and hence are not yet available. In order to get some earlier inputs we have evaluated the performance of a commercial version of the CCD47-20 (CCD47-20-339 ser.nr. 11203-02-03). Figure 11 shows the results of noise and gain measurements (using 5.9 keV X-rays), from which the operating point of the amplifiers has been derived. At the nominal operating conditions, the sensitivity of the gain to variations of the bias voltages has been measured and the results are listed in Table 4. These sensitivities are relevant in relation to the required stability of the bias voltages provided by the CHEOPS flight electronics. Figure 12 (left panel) shows the measured CTI at 200 kHz pixel rate and T=203K as a function of X-ray photon density in the test images. The measured CTI values for serial and parallel transfer at the reference photon density of 100 pixels/photon are found well within the requirement of $<5x10^{-6}$. The right hand panel of Figure 12 shows a photon transfer curve from which the conversion gain (used for QE measurements discussed below) and the full well capacity (FWC) are derived. The photon transfer curve is slightly non-linear due to charge redistribution, resulting in an apparent dependence of the gain on the signal. We use the zero-signal gain as the true gain. The FWC is derived as 105000 electrons.

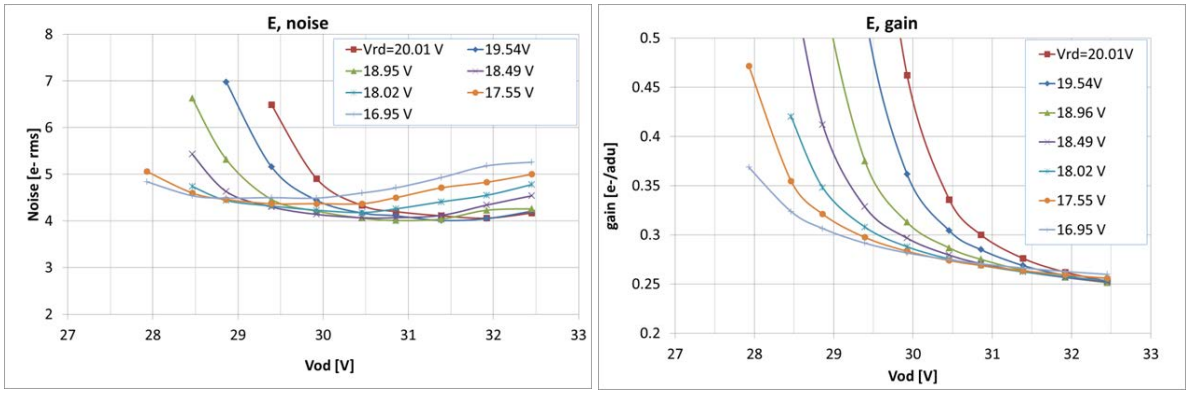

Figure 11: Left: readout noise (at 100 kHz pixel rate) and Right: conversion gain as function of reset drain voltage and output drain voltage for the one of the amplifiers on CCD47-20-339 ser.nr. 11203-02-03.

Table 4: Sensitivity (in ppm/mV) of the conversion gain of the two amplifiers to changes in bias voltages, at the nominal bias voltages

	VRD (18.5V)	VOD (31.5V)	VOG (3.0V)	Vss (9.5V)
E	7	-50	7	33
F	6	-49	8	32

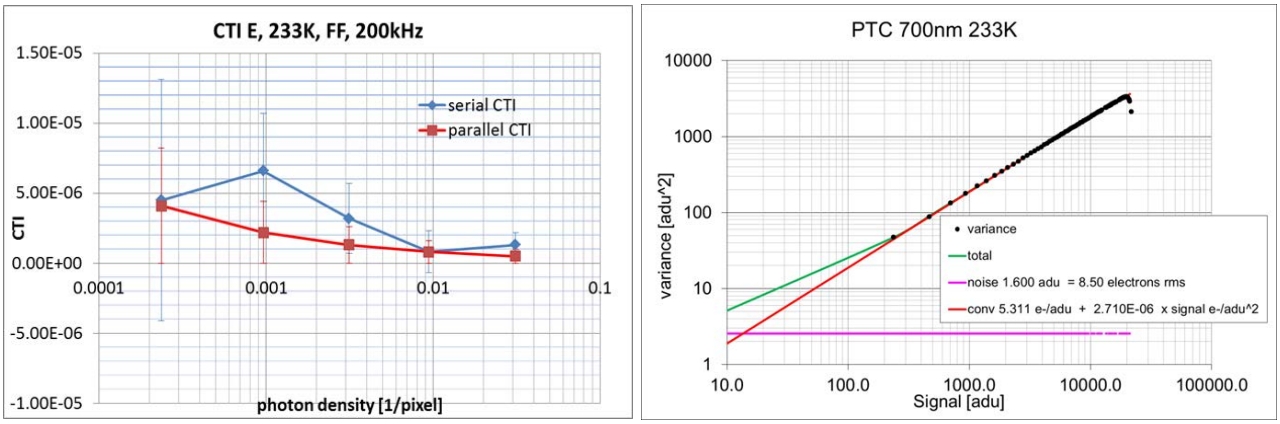

Figure 12: Left: CTI (at 200 kHz pixel rate, T=233K). Right: photon transfer curve.

The dark current has been measured as a function of temperature and, at the nominal operating temperature T=233K, as function of substrate voltage Vss, see Figure 13. The latter graph confirms the inverted mode operation of the device for

substrate voltages Vss>8V. At Vss=9.5V, the recommended operating point by e2v, the dark current is compliant with the required 0.1 e-/pixel/s, but further suppression of the dark current is possible at higher values of Vss. However, at these higher substrate voltages, a strong and non-uniform collapse of the FWC is observed.

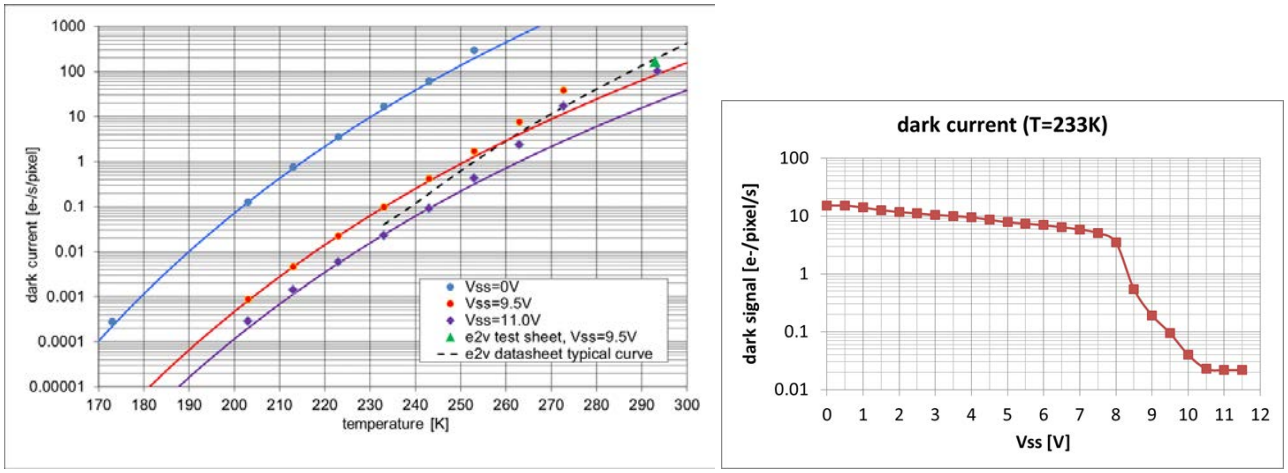

Figure 13: Left: Measured dark current versus temperature for 3 different values of Vss. Right: dark current versus substrate voltage Vss at T=233K.

The QE has been measured over the wavelength range of 400-1050 nm, for 4 temperatures between 178K and 253K, see Figure 14. Again , the sensitivity of the QE on temperature at the CHEOPS operating temperature T=233K) is derived from these data and, together with the sensitivity of CCD gain (1.1 ppm/mK) and of measured signal, is shown in the right panel of Figure 14. The results are in good agreement with calibrations performed on similar CCDs used for the COROT mission [19]. The wavelength dependent sensitivity of the measured signal has been convoluted with template star spectra of stars with different effective temperatures to find the sensitivity for different star types. The magnitude of the variation of the measured photometric signal of such stars, for a CCD temperature variation on 10 mK (as currently budgetted for CHEOPS) is shown in Figure 15. Clearly, the variations remain well within the allocated 10 ppm noise contribution from CCD temperature variations in the total photometry error budget [7].

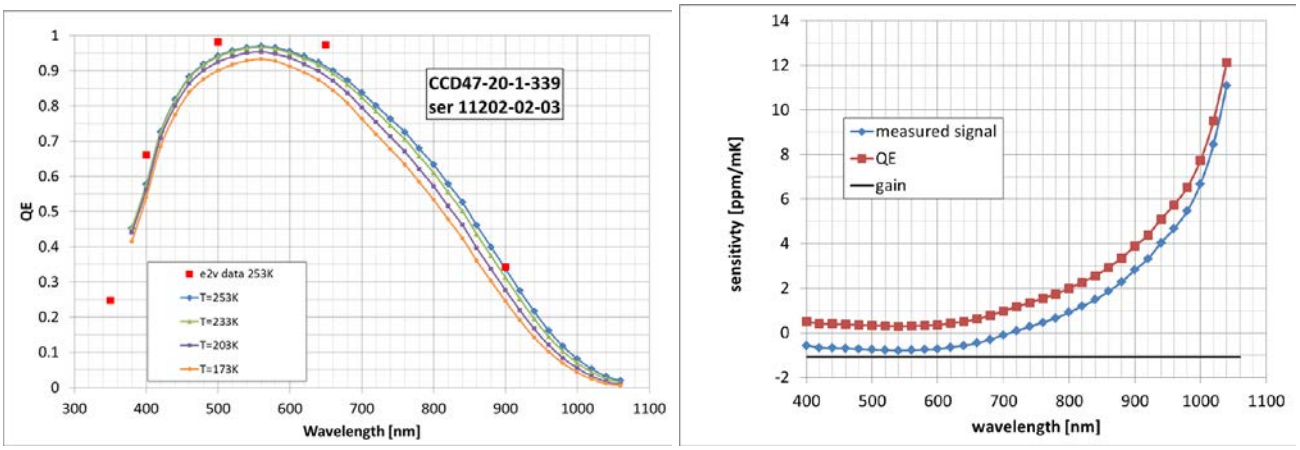

Figure 14: measured QE versus wavelength at 4 different temperatures. Right: The sensitivity of QE, gain and measured signal on temperature at T=233K.

Finally, flat field measurements have been performed at wavelengths between 400-1000nm, see Figure 16. The PRNU is dominated by the residual step pattern of the back-side laser annealing procedure. This pattern is most prominent at the shortest wavelengths, for which the photon absorption depth is very shallow, but remain visible up to the longest wavelengths. Such measurements are necessary to allow for correction of the combined effect of spacecraft residual jitter and CCD PRNU on the photometric signal. While a statistic accuracy of 0.1% is easily achievable at each individual

wavelength, the variation of the amplitude of the annealing pattern with wavelength requires calibration at a dense grid of wavelengths. Preliminary estimates, derived from simulations which include the spacecraft jitter, the CHEOPS PSF (diameter of ~ 30 pixels) and these flat fields, suggest that a grid of ~ 20nm will be needed, at least in the short wavelength range.

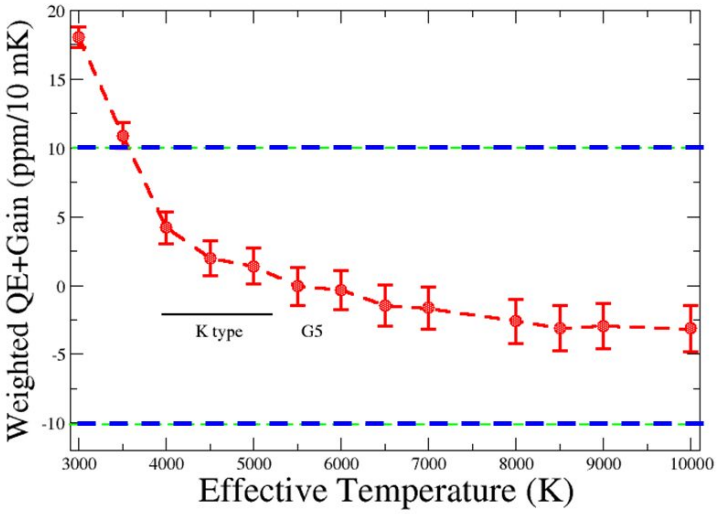

Figure 15: calculated sensitivity of the measured photometric signal for 10 mK temperature variations as a function of effective star temperature, due to gain and QE variations of the CCD. The blue dashed lines indicate the 10 ppm contribution for this effect which is included in the CHEOPS photometry error budget.

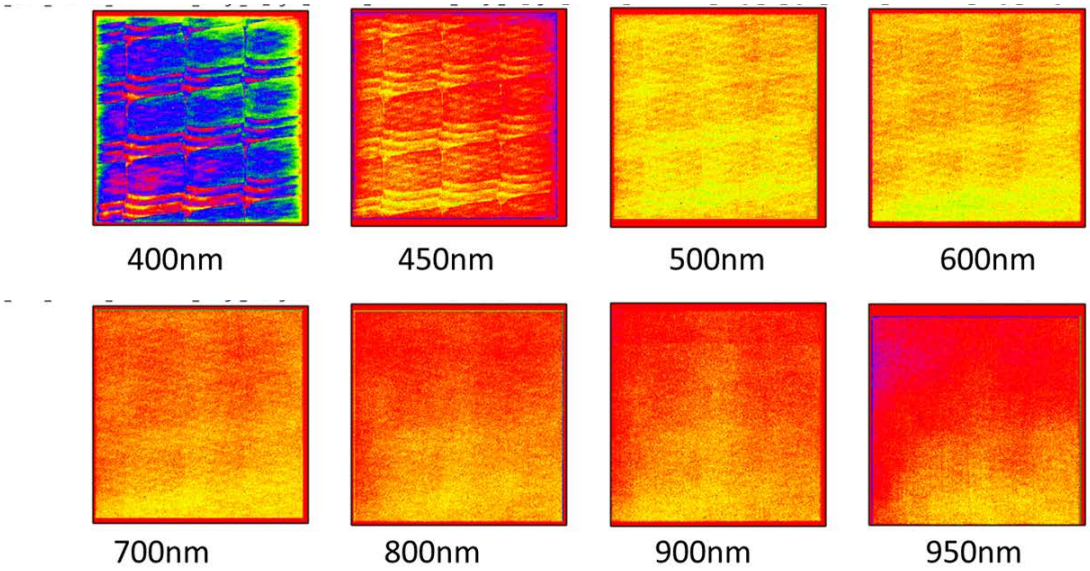

Figure 16: flat fields at wavelengths between 400-950 nm.

7. SUMMARY

Many of ESA's astronomy missions use CCDs as their principal detectors. Usually, ESA is responsible for the development and procurement of the CCDs, even if the instruments they reside in are provided by instrument consortia. As part of our role to support Science missions in various stages of their development and deployment, we operate a versatile CCD test bench, that can address mission specific performance issues. Examples include the EUCLID mission, for which the degradation of its ability to measure accurate shapes of galaxies by radiation damaged is investigated. For

other future missions such as PLATO and CHEOPS, both of which rely on accurate photometry with CCDs, we have investigated the basic performance of the CCDs. In particular, we have characterized the temperature dependence of gain and QE and evaluated the sensitivity of the photometric signal to changes in CCD temperature. This information provides valuable input to the noise budgets and calibration requirements of such missions.

REFERENCES

[1] den Herder, J.W., et al., "The Reflection Grating Spectrometer on board XMM-Newton," Astronomy and Astrophysics 365, L7-L17 (2001).

[2] Turner, M.J.L., et al., "The European Photon Imaging Camera on XMM-Newton: The MOS cameras," Astronomy and Astrophysics 365, L27-L35 (2001) .

[3] Kohley, R., et al., "The radiation environment at L2 as seen by Gaia," to be published in proceedings of SPIE 9154, (2014).

[4] Laureijs, R., et al., "Euclid: ESA's mission to map the geometry of the universe," Proceedings of SPIE 8442, 84420T, (2012)

[5] Cropper, M., et al. "VIS: the visible imager for Euclid," Proceedings of SPIE 8442, 84420V (2012).

[6] Stankov, A. et al., "Definition phase activities for ESA's Cosmic Vision mission PLATO," Proceedings of SPIE 7731, 77311M (2010)

[7] Fortier, A. et al., "CHEOPS: a space telescope for ultra-high precision photometry of exoplanet transits," to be published in proceedings of SPIE 9143, (2014).

[8] Verhoeve, P., et al., "ESA's CCD test bench for the Euclid visible channel," SPIE proceedings 8453, 845322 (2012).

[9] Crouzet, P.-E., et al., "Test set up description and performances for HAWAII-2RG detector characterization at ESTEC," Proceedings of SPIE, 8453, 845329 (2012).

[10] Crouzet, P.-E., et al., "Quantum efficiency test set up performances for NIR detector characterization at ESTEC," to be published in proceedings of SPIE 9154, (2014).

[11] Endicott, J., et al., "Charge-coupled devices for the ESA Euclid M-Class Mission," Proceedings of SPIE, vol. 8453, 845303 (2012)

[12] Verhoeve, P., et al., "Characterisation of CCDs for the EUCLID VIS channel," presented at Scientific Detector Workshop 2013, 7-13 October 2013, Florence, Italy, to be published in the proceedings of SDW2013, (2014).

[13] Hall, D., et al., "Modelling charge transfer in a radiation damaged charge coupled device for Euclid", Proceedings of SPIE 8453, 845315 (2012).

[14] Gow, J.P.D., et al., "Assessment of proton radiation-induced charge transfer inefficiency in the CCD273 detector for the Euclid Dark Energy Mission," Proceedings of SPIE 8453, 845316 (2012).

[15] Murray, N., et al., "Mitigating radiation-induced charge transfer inefficiency in full-frame CCD applications by 'pumping' traps," Proceedings of SPIE 8453, 845317 (2012).

[16] Prod'homme,T., et al., "A comparative study of charge transfer inefficiency value and trap parameter determination techniques making use of an irradiated ESA-Euclid prototype CCD," to be published in proceedings of SPIE 9154, (2014).

[17] Prod'homme, T., et al., "Laboratory simulation of Euclid-like sky images to study the impact of CCD radiation damage on weak gravitational lensing," to be published in proceedings of SPIE 9154, (2014).

[18] Endicott, J., Walker, A., Bowring, S., Turner, P., Allen, D., Piersanti, O., Short, A., Walton, D., "Charge-coupled devices for the ESA PLATO M-class Mission," Proceedings of SPIE 8453, 84531J (2012)

[19] Bernardi, P., Lapeyrere, V., Buey, J.-T., Parisot, J., Schmidt, R., Leruyet, B., "Performance of the COROT CCD for high-accuracy photometry," In: Second Eddington Workshop: Stellar structure and habitable planet finding, 9 - 11 April 2003, Palermo, Italy. Edited by F. Favata, S. Aigrain and A. Wilson. ESA SP-538, Noordwijk: ESA Publications Division, ISBN 92-9092-848-4, 191–195 (2004).